COMSOL
CONFERENCE
2023 MUNICH

Numerical simulation of Laser Ignition of Metallic Rods under Oxygen Pressure

S. TOUZOUIRT[1], J. DALIGAULT[2], M. DAL[2], N. GALIENNE[1], M. RIDLOVA[1], F. COSTE[2]
1. Campus Innovation Paris d'Air Liquide, 1 Chem. de la Prte des Loges, 78350 Les Loges-en-Josas, France.
2. PIMM Laboratory, Arts et Métiers Institute of Technology (Paris), CNRS, CNAM, HESAM University, 151 Boulevard de l'Hôpital, 75013 Paris, France.

Abstract
The presence of oxygen in installations involving metallic components can influence their flammability threshold and thus lead to combustion ignitions. In order to classify metals according to their degree of flammability many studies have been conducted leading to the creation of ASTM G124-18 standardized flammability test for metals. The aim of this work is to develop a numerical equivalent for this test, including laser ignition as heat source and involving heat transfer, fluid flows, and diffusion of chemical species, coupled under a Phase Field approach and enhanced with an adaptative mesh refinement in order to describe the whole rod combustion process.
Keywords: Phase Field, Adaptive Mesh Refinement, high temperature combustion, Oxygen fire phenomena, ASTM G124-18.

1. Introduction

When subjected to a rich oxygen atmosphere flammability of metallic components can be influenced, and if a certain amount of energy is added to the equation, either from particle collision with the metallic walls or from friction between the various parts, combustion ignitions can be triggered. The resulting thermal energy transmitted to the container walls affects their mechanical properties, causing them to deform or even to crack because of the pressure gradient between the internal and the external media, leading to a potential loss of containment.
In order to develop more suitable designs for equipment in oxygen installations many studies have been conducted, aiming to characterize the flammability of different metals under given temperature and oxygen pressure test conditions, to define threshold limits beyond which a combustion ignition would occur leading to a total or partial consumption of the material.
These studies led to the creation of the ASTM G124-18 test, a standardized test method for the classification of the metals according to their flammability. In this test, a rod made from the required material is used and to which thermal energy is supplied via an igniter-promoter association whose role is to trigger a combustion ignition, followed by the burning of a given length of the rod, in order to consider the combustion as self-sustained and for the test to be validated.
Many other studies have been conducted in order to study the effect of different parameters such as material coating [1], the testing of various materials in flowing oxygen [2], preheating of the material [3] or even testing different shapes, geometries and dimensions of the sample [4] [5] [6].
In a previous contribution to the ASTM G124-18 test [7] a change of the heat source was proposed, switching from an igniter-promoter assembly to a laser. First, this version of the test would have a higher reproducibility as the laser beam will be directed by a robot, unlike winding the igniter wire around the rod manually. The amount of energy provided to the rod by the laser will also be known and even control its distribution on the impact surface of the rod is accomplished.
Given the fact that this application is a multyphysical case that includes numerous phenomena from different physics, which are all taking place at high temperature and are strongly coupled, experimental exploration of this case remains difficult. Thanks to progresses made in Computationnal Fluid Dynamics (CFD) numerical simulation could help overcome these difficulties, and thus should be one of the major tools for oxygen fire understanding.
Several models have been developed in order to reproduce numerically the whole process of rod combustion, using different numeric schemes or mesh approaches [7] [8].
In our work, the model considers heat transfers, fluid flows and diffusion of the chemical species between solid, gas and liquid phases, all of that coupled under a Phase Field approach, enhanced with an Adaptive Mesh Refinement, to reproduce accurately the significant morphological changes in the interface and also the fall of metallic liquid drops.
In this paper, the mathematical/physical model will be described, then results will be presented with an accompanying discussion, and finally a conclusion and outlook on the next steps will be provided.

2. Modeling

2.1. Physical and process parameters

The equations describing the different coupled physics are computed using COMSOL Multiphysics V6.1, using the finite element method.
The rod used is made with pure iron. The implemented values of its physical parameters are given in the following table [9]:

Table 1 – Physical parameters

Parameter	Symbol [unit]	Value
Ambient temperature	T_0 [K]	293.15
Melting point	T_f [K]	1723
Boiling point	T_v [K]	3173
Melting latent heat	L_f [J.kg^{-1}]	$2.5 \cdot 10^5$
Evaporation latent heat	L_v [J.kg^{-1}]	$6.4 \cdot 10^6$
Surface tension	γ [N.m^{-1}]	1.5
Surface tension variation	$\frac{d\gamma}{dT}$ [N.m^{-1}K^{-1}]	10^{-4}
Iron solid viscosity	η_s [Pa.s]	10^5
Iron liquid viscosity	η_l [Pa.s]	10^{-3}
Iron density	ρ [kg.m^{-3}]	7860
Iron heat capacity	C_p [J.kg^{-1}.K^{-1}]	420
Iron heat conductivity	K [W.m^{-1}.K^{-1}]	40
Temperature range between the solidus and liquidus	ΔT [K]	20

As shown in Table 1, at this step of the study, the material properties are assumed to be constant. Concerning process parameters, a relatively low power for the laser was used in order to avoid instabilities [10] and to have a smoother repartition of the absorbed energy along the rod. On top of that, the radius of the laser beam is taken to be equal to that of the sample to ensure energy is deposited within the perimeter of the rod's base. The exact values for the experimentally measured parameters are given in Table 2.

Table 2 – Process parameters

Parameter	Symbol [unit]	Value
Power	P_{laser} [W]	1000
Beam radius	r_0 [mm]	1.5
Pulse duration	t_{laser} [s]	0.5

2.2. Geometry

Given the cylindrical geometry of the sample and the fact that the energy deposit is occurring only at its base, we use an axisymmetric configuration for our simulations [10], as shown in Figure 1.

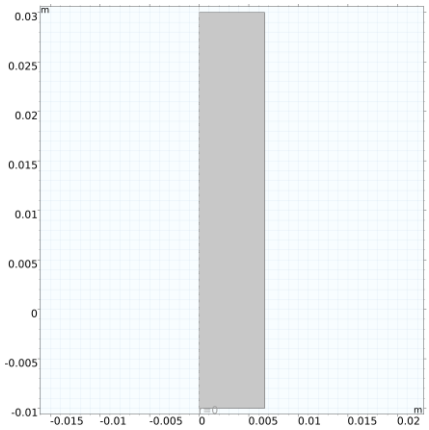

Figure 1. Geometry

2.3. Phase Field Approach

Given the fact that our application includes the formation, the ascension along the rod, and the detachment of a liquid metal drop and thus important morphological changes in the interface, we choose to use an Eulerian approach with a fixed mesh. To decide which of the methods proposed by COMSOL Multiphysics is the most suitable for our study, we take into account the fact that surface tension effects are of a major interest in our case, as they depend on temperature, and characterize the drop formation, shape and detachment. Thus, the Phase Field approach seems to be the most convenient for our study.
The Phase Field approach is based on the Cahn-Hilliard equation. The equations are solved as a combination of two 2nd order equations, instead of the original 4th order equation:

$$\frac{\partial \emptyset}{\partial t} + \vec{u}.\vec{\nabla}\emptyset = \vec{\nabla}.\left(\frac{3}{2\sqrt{2}}\sigma\epsilon\chi\vec{\nabla}\psi\right) \qquad (20)$$

$$\psi = -\vec{\nabla}.\left(\epsilon^2\vec{\nabla}\emptyset\right) + (\emptyset^2 - 1)\emptyset \qquad (21)$$

Where ϕ is the phase field variable, ε the interface thickness parameter, κ the mobility, and λ the mixing energy density.
The principle is simple, instead of having a sharp interface separating our two domains like in the classical sharp interfaces approaches, we track the dynamic of a diffusive interface. The diffusive interface allows us to have a smoothed transition in the parameters values between the two phases, across its thickness and thus increase the stability and the convergence of the model.
As said before, the Phase Field approach is a suited method when we have surface tension phenomena as it's characteristic parameters can directly be linked to the surface tension coefficient:

$$\gamma = \frac{2\sqrt{2}}{3}\frac{\lambda}{\varepsilon} \qquad (22)$$

The other physical properties of each phase are also linked to the phase field variable, this is done using linear relations, through the variable $\emptyset$ which will work as a phase identification parameter taking the value 1 in the iron rod and -1 in the gas.

As all the variables are linked, assigning them the right value or model and choosing the right mesh size is a major criterion in the convergence and the accuracy of the Phase Field approach.

2.4. The thermal problem

Heat transfer is one of the fundamental physics in our study as it allows us to follow the evolution of the temperature over time and to quantify the different energies involved. To do so, we solve the energy equation:

$$\rho c_{p\,eq}\frac{\partial T}{\partial t} + \rho c_{p\,eq}\vec{u}.\,\vec{\nabla}T = \vec{\nabla}.\left(k\vec{\nabla}T\right) + S \qquad (1)$$

Where T is the temperature, $\vec{u}$ the fluid velocity vector, ρ the density, k the thermal conductivity, S the volume source terms, and $c_{p\,eq}$ an specific heat. All the physical parameters in the previous equation will depend on the phase field variable ϕ.
The use of an equivalent specific heat allows us to consider the melting phase change and is given by the following expression [7]:

$$c_{p\,eq} = c_p(T) + \delta c_p * L_f \qquad (2)$$

With c_p (T) the specific heat evolution with temperature, L_f the latent heat of melting, and δc_p given by [7]:

$$\delta c_p = \frac{1}{\Delta T\sqrt{\pi}} e^{-\left(\frac{T-T_{fusion}}{\Delta T}\right)^2} \qquad (3)$$

With T_{fusion} the temperature corresponding to the melting point of the metal.
As for the source term, including all the flux acting at the interface and the source from the chemical reaction. The absorbed flux is given by:

$$\varphi_{absorbed} = \frac{\alpha P}{A_b} \quad for \quad r_{laser} \leq r_{rod} \qquad (4)$$

With α the absorptivity of the metal, P the laser power, and A_b the base area of the metallic rod, r_{laser} the radius of the laser beam and r_{rod} the radius of the rod.
As the two phases (metal and gas) are simulated, the only losses to consider are radiative:

$$\varphi_{radiation} = e\sigma(T^4 - T_0^4) \qquad (5)$$

With e the emissivity of the sample and σ the constant of Stefan-Boltzmann.
The heat loss due to evaporation of the rod is given by:

$$\varphi_{evaporation} = \dot{m} \cdot L_v \qquad (7)$$

With $\dot{m}$ the mass debit of the evaporated material computed with [11]:

$$\dot{m} = (1-\beta)\sqrt{\frac{M}{2\pi RT}P_{sat}^{Clapeyron}} \qquad (8)$$

Where β is a factor used to characterize the fraction of re-condensated matter. The Clapeyron pressure is given by [10]:

$$P_{sat}^{Clapeyron} = p_0 e^{\frac{L_v M}{RT_{vap}}\left(1-\frac{T_{vap}}{T}\right)} \qquad (9)$$

Finally, the heat created by the chemical reaction is given by [7]:

$$S_{reaction} = h_f \cdot c_o \cdot c_{Fe} \cdot e^{-\frac{E}{RT}} \qquad (10)$$

With h_f the enthalpy of formation of the oxide, c_o and c_{Fe} oxygen and iron concentrations coming from the resolution of chemical species quations , and E the activation energy of the reaction.

As for the initial conditions, we impose the ambient temperature as an initial temperature in all the domains. Given our configuration, we also assume that our boundary conditions are of little importance.

2.5. The fluid flow problem

The fluid flow will play an essential role after the appearance of the metal's molten phase, we model it using the Navier-Stokes equations for an incompressible fluid:

$$\vec{\nabla}.\vec{u} = 0 \qquad (11)$$

$$\rho\frac{\partial \vec{u}}{\partial t} + \rho(\vec{u}.\vec{\nabla})\vec{u} = \vec{\nabla}.\left[-p\bar{\bar{I}} + \mu\left(\vec{\nabla}\vec{u} + \vec{\nabla}\vec{u}^T\right)\right] + \rho\vec{g}\beta\left(T - T_{fusion}\right) + \vec{F} \qquad (12)$$

Where ρ is the density, u the fluid velocity vector, p the pressure, μ the dynamic viscosity, $\vec{g}$ the acceleration of gravity, β the thermo-density coefficient and $\vec{F}$ the volume source term.
When liquid metal in the bottom of the rod reaches vaporization temperature metal vapor will be generated and released, which will create a recoil pressure which in turn will tend to apply a force towards the inside of the bubble [10]:

$$P^{recoil} = \frac{1+\beta}{2}\cdot\left(P_{sat}^{Clapeyron}(T) - p_{ext}\right) \qquad (13)$$

Where p_{ext} is the ambient pressure.
In order to counterbalance the deformation of the interface imposed by the recoil pressure and thus bring back the system to a configuration of minimum energy, capillary effects tends to act on the normal direction through the Laplace pressure, creating a force [10]:

$$\vec{F}^{Laplace} = \gamma\left(\vec{\nabla}_s \cdot \vec{n}\right)\vec{n} \qquad (14)$$

Where ∇_s is the surface gradient, and n is the normal vector pointing in the outward direction from the interface.
The variation with temperature of the surface tension coefficient generates a tangential effect known as Marangoni effect which creates a sort of convection motion inside the liquid metal, the force generating this motion can be described by [12]:

$$\vec{F}^{Marangoni} = \vec{\nabla}_s\gamma \qquad (15)$$

We initially impose a zero field for velocity and pressure in all the domains, keeping the same assumption as before for the boundary conditions.

2.6. Diffusion of chemical species problem:

As the energy delivered from this chemical reaction is one of the principal energy sources in our study and the diffusion of oxygen inside the sample can be viewed as one of the main parameters into the process of rod consumption, the chemical mechanisms and kinetics involved in the metallic rod combustion are essential to our study. To model the transport of each species in the different phases, we use Fick's second law:

$$\frac{\partial c_i}{\partial t} + \vec{\nabla}.\,\vec{j_i} + \vec{u_i}.\vec{\nabla}c_i = R_c \qquad (16)$$

With $\vec{j}$ the molar flux given by Fick's first law:

$$\vec{j_i} = -D_i.\overrightarrow{\nabla c_i} \qquad (17)$$

With D_i the diffusivity coefficient of the element i, $\overrightarrow{\nabla c_i}$ is its concentration gradient in a given medium, and R_c is the reaction rate. In our study, it corresponds to the rate at which the iron oxyde is created, it is described by an experimentally determined relation [7]:

$$R_c = c_{Fe}c_{o2}v(t) \qquad (18)$$

Where c_{Fe} and c_o are the concentrations of iron and oxygen respectively, and v(T) is the velocity parameter of the relation, given by an Arrhenius law [7]:

$$v(T) = Ae^{-\frac{E}{RT}} \qquad (19)$$

Where A is the frequency parameter, it takes into account the frequency at which atoms collide, E is the activation energy of the iron oxide and R is the gas constant.

For the initial conditions, we impose finite values of the concentrations for both iron and oxygen in the corresponding phase for each element, keeping also the same assumption as before for the boundary conditions.

3. Numerical Approach:

3.1. Interface conditions modelling:

Although the smoothed interface is very advantageous in terms of interface management, we can't apply conditions to it. Instead, all surface conditions are considered as volume sources terms that only take place at the interface. We do that by using the delta function (δ) which is defined using the gradient of the phase field variable ∇ϕ. Thus, it will be zero in the bulk phases and will only have a value in the transition zone (interface thickness). The delta function is predefined in COMSOL as:

$$\delta = 6|\nabla\emptyset||\emptyset(1-\emptyset)| \qquad (23)$$

For example, for the heat flux absorbed from the laser:

$$S_{absorbed} = \varphi_{absorbed} \cdot \delta = \frac{\alpha P}{S} \cdot \delta \qquad (24)$$

3.2. Mesh and Mesh Refinement:

As for the mesh, we use a combination of an initial mesh with an adaptive mesh refinement approach. This allows us to use a relative coarse but still precise mesh at the beginning of the calculations and then refine it in areas of interest, instead of using a mesh that would have been too expensive in terms of calculation cost, and while maintaining a good precision in the computations.
For the initial mesh, we use a structured quadrilateral mesh on all the geometry, for which a custom maximal element size is used. The meshed geometry is shown in the figure below:

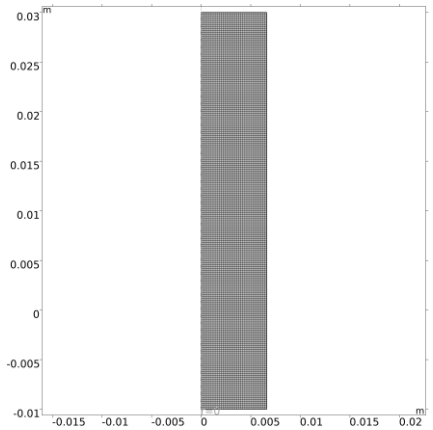

Figure 2. Mesh

For the mesh refinement, we use the time-interval length feature in COMSOL which allows us to define the simulation time before a refinement of the mesh takes place. We also use the interval reduction factor which decreases the value of the time-interval length and thus increases the number of refinements over time. Knowing the study and values of variables like the interface thickness and their ratio to the initial mesh we choose to consider a sufficient fixed number of refinements, and impose it with the maximal number of refinements feature in COMSOL.
As for the regions where the refinement occurs we choose both the interface and the regions containing melting iron as they are of most interest in our study. We impose the refinement condition at the interface using the δ-function:

$$\frac{\delta}{\max(\delta)} \qquad (25)$$

The condition to refine inside the molten iron is achieved by using both ϕ to indicate that we are in the metal phase and the liquid fraction to ensure that we only remesh the molten part

$$pf.Vf2 \cdot (lf > 0) \qquad (26)$$

With lf the liquid fraction and $pf.Vf2$ the metal phase indicator

The mesh after each refinement is saved in order to track its evolution over the course of the simulation, and the results will be shown in the results section.
For the numerical resolution, we use a direct approach to solve the linearized problem, including a PARDISO solver for the phase field variables, heat transfer variables, and fluid flow variables. For the time-dependent variables, we use an α-generalized solver.

4. Results

For the first simulations, the aim was to run tests to find the right value for the characteristic numerical parameters of the Phase Field, to ensure a good stability and convergence, which could lead us to the detachment of the molten iron drop from the rod, as the model developed in a previous thesis, where an ALE (Arbitrary Lagrange Euler) was used, was unable to reach this stage [Khaled].
In order to do that, and for calculations cost reasons, first models considered just the heat transfer and fluid flow, being the physical prerequisites for the formation and detachment of the drop. Figure 3 shows the results for these first tests:

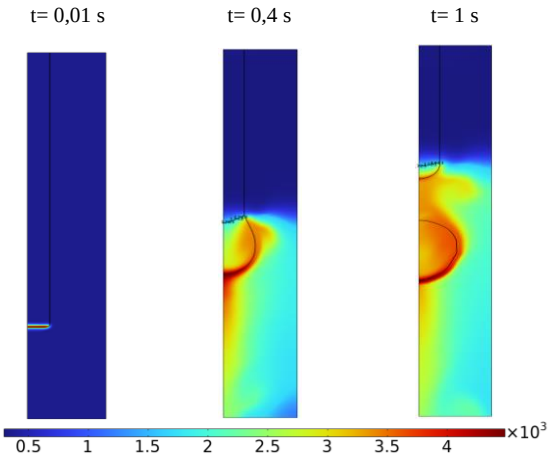

Figure 3. Temperature field evolution without oxydation.

As expected, the Phase Field approach is well suited for the important morphological changes in the interface, and allows us to attain the drop detachment from the rod.
After the drop test was passed, we created the final model, including the remaining physic, the transport of diluted species, to model the transport of oxygen inside the iron rod, leading to the apparition of the oxide, controlled by the oxidation rate mentioned above, and thus reproduce the complete rod combustion process. The simulation results are illustrated in Figure 4.

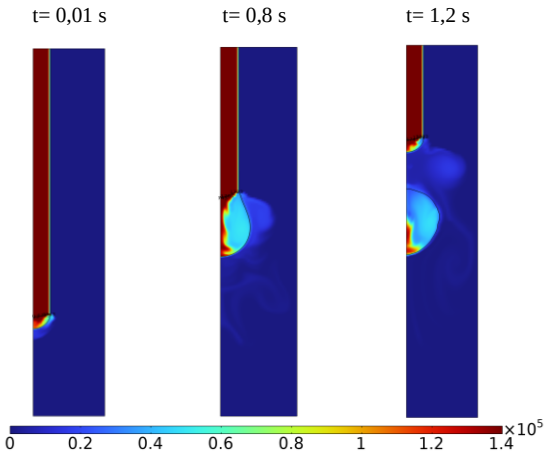

Figure 4. Iron concentration field evolution

We can clearly observe an increasing region in the molten part of the rod where the concentration of pure iron decreases, which we assume to correspond to iron oxide, resulting from oxygen diffusion in the iron matrix.
As this formulation is not yet complete, we can observe that we have a non-physical diffusion of iron inside oxygen, which will need a more in-depth description of the diffusivity coefficients.
To verify that the oxygen is actually diffusing inside the iron rod, we extract the oxygen concentration contours. The results are shown in Figure 5.

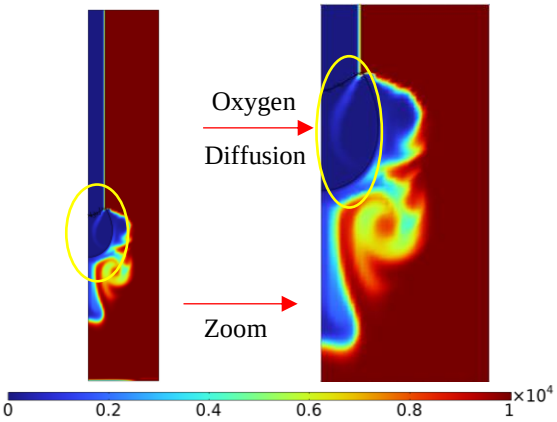

Figure 5. Oxygen concentration field evolution

The contours of oxygen concentration allows to verify that oxygen diffusion does indeed take place inside the rod, especially in the molten phase, which was predictable given that oxygen solubility and coefficient of diffusivity in liquid iron are greater than that in solid iron.
As stated earlier in this work, we also extract the mesh contours to check the effectiveness of the adaptative refinement method, as well as our choices for its characteristic parameters. These contours are illustrated in figure 6.

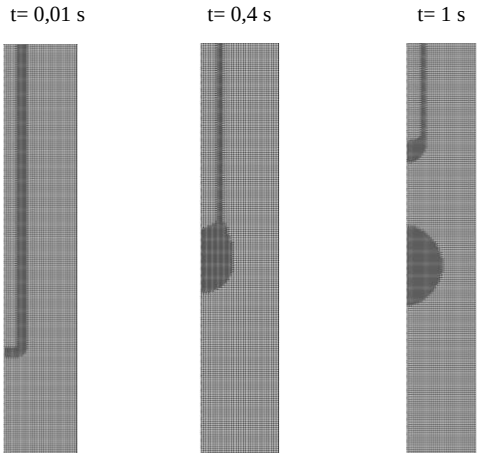

Figure 6. Evolution of the refined mesh

Refined mesh contours enable us to check that mesh refinement does indeed take place in the defined zones of interest, the interface and the molten zone of the iron rod. We can also observe that the refinement adapts also accurately to the dynamic of the rod combustion over time. In a more quantitative way, the mesh refining allows us to divide the number of degrees of freedom by around 4, from 241736 degree of freedom without refinement to 61472 with refinement, which corresponds to a non-negligible cost of calculation.

5. Conclusions

Although this work is in its early stages, we can nevertheless draw some conclusions from the results obtained. We were able to observe that the use of the phase field was well suited to our case, especially for managing the drop detachment. We were also able to verify the effectiveness of adaptative mesh refinement, which allows us to optimize our calculation cost by finely meshing only in areas of interest. Finally, we observed that we were able to include diffusion of oxygen inside the iron rode, even though the formulation is not complete, and still includes some non-physique results, like the diffusion of iron inside oxygen.

6. Outlooks

As for the next steps in our study, our main efforts will be focused on the determination of a precise expression for the diffusivity coefficients of each element in the different phases, including solubility of oxygen in solid and liquid iron and allowing us to get rid of the oxygen non-physical diffusivity in iron. We also aim to develop a model containing two separate Phase Fields, in order to simulate the creation of iron oxide as a phase apparition under given conditions. Our work will also include a sensitivity study for the physicial parameters in order to determine which are of major interest in our application, which will then be determined by inverse estimation methods combining experimental and numerical (COMSOL Optimization Module, MATLAB Livelink, …etc.) resources. These values will be then implemented in the model in order to carry out the experimental validation. Finally, the model will be transposed to geometries closer to those of real oxygen service facilities and for various alloys.

7. Bibliographie

[1] Binder, Chr & Kasch, T & Brock, T & Beck, Uwe & Weise, Matthias & Share, M. (2006). Promoted Combustion Testing of Pure and Ceramic-Coated Metals in High Pressure Oxygen by the Federal Institute of Materials Research and Testing (BAM). Journal of Astm International. 3. 10.1520/JAI13533.

[2] Forsyth, E., Maes, M.J., Stoltzfus, J.M., & Bachelier, F. (2003). Promoted Ignition and Burning Tests of Stainless Steel in Flowing and Nonflowing Oxygen.

[3] Engel, C., Herald, S.D., & Davis, S.E. (2013). *Promoted Metals Combustion at Ambient and Elevated Temperatures.*

[4] Binder, Chr & Kasch, T & Lehné, S & Beck, Uwe & Weise, Matthias & Sahre, M. (2006). *Combustion Tests Under High Pressure Oxygen: Promoted Ignition Combustion Test Versus Metallic Disk Ignition Test*. Journal of Astm International. 3. 10.1520/JAI13532.

[5] D. Wilson, E. Forsyth, M. Maes, J. Stoltzfus, A. International, A. S. for *Testing, and Materials, Modeling the Ignition of Large Diameter Rods and Pipes in Flowing Oxygen*. ASTM International, 2003.

[6] Steinberg, Theodore & Suvorovs, Terese & Ward, Nicholas & Wilson, Richard. (2006). *Effect of Sample Geometry on Regression Rate of the Melting Interface for Carbon Steel Burned in Oxygen*. Journal of ASTM International. 3. 10.1520/JAI13565.

[7] Muller, Maryse. (2013). *Investigation on Laser Initiation and Propagation of the Combustion of Mild Steel and Stainless Steel in an Oxygen Atmosphere.*

[8] Coste Frédéric, Ridlova Martina, Ayfi Khaled, Dal Morgan , Labegorre Bernard , Galliene Nicolas, Quintard Jacques, Fabbro Remy and Colson " *Laser Ignition of Metallic Rods and Discs in Gaseous Oxygen. A Complementary Approach to the Standard ASTM G-124 Test Method*. Under submission at 15*th International Symposium on Flammability and Sensitivity of Materials in Oxygen-Enriched Atmospheres*

[9] Kenneth C Mills,Fe -C Grey Cast Iron, Editor(s): Kenneth C Mills, In Woodhead Publishing Series in Metals and Surface

Engineering, *Recommended Values of Thermophysical Properties for Selected Commercial Alloys*, Woodhead Publishing, 2002, Pages 119-126, ISBN 9781855735699,

[10] V .Bruyere, C. Touvrey, P. Namy. *A Phase Field Approach to Model Laser Power Control in Spot Laser Welding*. COMSOL Conference in Cambridge, 2014.

[11] V. Fedorov and R. Moore, Effect of Laser Radiation on Absorbing Condensed Matter, ser. Proceedings of the Institute of General Physics, Academy of Sciences of the USSR. Nova Science, 1990.